

Spaceborne Polarimetric SAR Interferometry: Performance Analysis and Mission Concepts

Gerhard Krieger⁽¹⁾, Kostas Papathanassiou⁽¹⁾, Shane Cloude⁽²⁾, Alberto Moreira⁽¹⁾,
Hauke Fiedler⁽¹⁾, Michael Völker⁽³⁾

⁽¹⁾ *Microwaves and Radar Institute, German Aerospace Center (DLR), Germany*

⁽²⁾ *School of Electrical and Electronic Engineering, The University of Adelaide, Australia*

⁽³⁾ *EADS Astrium GmbH, Friedrichshafen, Germany*

ABSTRACT

This paper analyses the potentials and limitations of spaceborne fully polarimetric SAR interferometers. The analysis includes both conventional repeat pass mission scenarios like ALOS/PalSAR or TerraSAR-L, as well as single-pass mission scenarios like a fully-polarimetric Interferometric Cartwheel or TanDEM-X. The PolInSAR performance of the suggested scenarios will be analysed by introducing the new concept of a phase tube. This concept enables an optimization of the system parameters and a quantitative comparison between different sensor configurations. Furthermore, important aspects in the design of future PolInSAR sensors will be addressed and the benefits arising from the use of single pass sensor configurations will be demonstrated.

1. INTRODUCTION

Spaceborne polarimetric SAR interferometry enables quantitative measurements of important bio- and geophysical parameters of the Earth surface on a global scale. The potentials of polarimetric SAR interferometry for image segmentation, classification, and vegetation measurements have successfully been demonstrated in many airborne SAR campaigns. In the future, the PolInSAR technique is expected to enable powerful remote sensing data products for a wide range of forest, agriculture, land cover, and land ice applications. However, care must be taken in transforming the very promising results achieved with airborne SAR sensors to the spaceborne case which has its own peculiarities like an increased NESZ, higher range and azimuth ambiguities, and lower incident angles. The major goal of this paper is hence a mission and performance analysis to assess the potentials and limitations of spaceborne PolInSAR sensors. For this, we consider both conventional repeat pass mission scenarios employing a single satellite (Section 2) as well as single pass mission scenarios which enable a polarimetric and interferometric data acquisition without temporal decorrelation (Section 3). The performance analysis will be based on the three application scenarios summarised in Table 1. Most of the data in this table have been derived from information available in the literature, but slight modifications had to be made to adapt the scenarios to the spaceborne case. An example is the maximum incident angle of 35° which can be regarded as an upper limit for most fully polarimetric spaceborne SAR sensors to be considered in the subsequent sections.

	L-Band (Forest)	C-Band (Agriculture)	X-Band (Agriculture)
Vegetation	Scots Pine Forest	Wheat (LAI of 3.5)	Wheat
Vegetation Height	20 m	0.7 m	0.6 m
Scattering Coefficient	$\sigma_0 > -11 \text{ dBm}^2/\text{m}^2$ (co-pol) $\sigma_0 > -14 \text{ dBm}^2/\text{m}^2$ (cross-pol)	$\sigma_0 > -15 \text{ dBm}^2/\text{m}^2$ (co-pol), $\sigma_0 > -18 \text{ dBm}^2/\text{m}^2$ (cross-pol)	$\sigma_0 > -10 \text{ dBm}^2/\text{m}^2$ (co-pol), $\sigma_0 > -13 \text{ dBm}^2/\text{m}^2$ (cross-pol)
Incident Angle	35°	35°	35°
Extinction	0.3 dB/m	2 dB/m	10 dB/m
Ground-to-Volume Ratios	-26 dB < μ < -2 dB	-18 dB < μ < 8 dB	-6 dB < μ < 0 dB
Independent Post Spacing	50 m x 50 m	30 m x 30 m	30 m x 30 m
Remarks and References	adapted from [3], see also [10]	adapted from [4] and [5], see also [11]	poor X-band support in literature, some hints in [6][7][8]

Table 1. Parameters of reference scenarios for L-, C-, and X-band.

2. REPEAT PASS MISSION SCENARIOS

This section investigates the achievable performance of repeat pass PolInSAR mission scenarios where the polarimetric and interferometric data are acquired with a single satellite in subsequent passes. The use of different satellite passes for PolInSAR data collection will imply a significant time lag of several days up to several weeks between the acquisitions of the two interferometric channels. Hence, temporal decorrelation is expected to become a major issue, especially at shorter wavelengths. We have therefore limited the analyses in this section to TerraSAR-L and ALOS/PalSAR. The left columns of Table 2 summarize the major system parameters of these two L-band satellites. Note that all parameters of Table 2 have been derived from the open literature and may hence only be regarded as first order approximations.

	TerraSAR-L	ALOS	Radarsat 2	TerraSAR-X
Wavelength	0.238 m (L-band)	0.236 m (L-band)	0.0555 m (C-band)	0.031 m (X-band)
Chirp Bandwidth	80 MHz	14 MHz (full pol.)	30 (100) MHz	150 MHz
Peak Power (radiated)	4740 W	2000 W	1650 W	2260 W
Duty Cycle	3,5 % (7%/2)	3,5 % (7%/2)	3 % (6%/2)	9 % (18%/2)
Rx Noise Figure	2.5 dB	4 dB	4 dB	4.5 dB
Losses (atmosphere, swath, proc., ...)	< 5 dB (for 40 km swath)	< 5 dB (for 40 km swath)	3 dB (25 km swath)	6 dB (split antenna !)
Antenna Size	11 m x 2.86 m	8.9 m x 3.1 m	15 m x 1.5 m	4.8 m x 0.7 m
Co-Registration	1/10 pixel	1/10 pixel	1/10 pixel	1/10 pixel
Quantisation (BAQ)	4 bit	4 bit	4 bit	4 bit
Orbit Height	629 km	691 km	798 km	514 km
Repeat Cycle	14 days	46 days	24 days	11 days

Table 2: System parameters for performance analysis

The performance analysis is based on a multiplicative coherence model where the total coherence is given by

$$\tilde{\gamma}_{tot} = \gamma_{SNR} \cdot \gamma_{Quant} \cdot \gamma_{Amb} \cdot \gamma_{Coreg} \cdot \gamma_{Geo} \cdot \gamma_{Az} \cdot \tilde{\gamma}_{Vol} \cdot \tilde{\gamma}_{Temp}$$

The right hand side describes the individual decorrelation contributions (cf. [10] for a more detailed discussion):

γ_{SNR} :	Finite SNR due to Thermal Noise (scalar contribution)
γ_{Quant} :	Quantization Errors (scalar contribution)
γ_{Amb} :	Range and Azimuth Ambiguities (scalar contribution)
γ_{Coreg} :	Co-Registration and Processing Errors (scalar contribution)
γ_{Geo} :	Baseline Decorrelation (scalar contribution)
γ_{Az} :	Decorrelation due to Doppler Shift (scalar contribution)
$\tilde{\gamma}_{Vol}$:	Volume Decorrelation (complex contribution)
$\tilde{\gamma}_{Temp}$:	Temporal Decorrelation (complex contribution)

Volume decorrelation $\tilde{\gamma}_{Vol}$ is in the following described by the random volume over ground model

$$\tilde{\gamma}_{vol}(\bar{w}) = \exp(i\phi_0) \frac{\tilde{\gamma}_V + \mu(\bar{w})}{1 + \mu(\bar{w})},$$

where ϕ_0 is the ground topography phase, $\mu(\bar{w})$ is the ground-to-volume scattering ratio for polarisation \bar{w} , and $\tilde{\gamma}_V$ denotes the coherence for the volume alone [1][2]. From the estimated coherence, phase and height errors have been derived assuming an independent post spacing of 50 m x 50 m. The results of the performance analysis are summarised in Fig. 1 for ALOS (left) and TerraSAR-L (right) in form of the so-called phase tubes which indicate different interferometric errors relative to the mean height of the phase centre [10]. The green dashed lines in the middle of the tubes show the variation of the vertical phase centre as a function of the ground-to-volume ratio $\mu(\bar{w})$. The green tubes indicate the standard deviation of the estimated errors ($\pm\sigma$) due to volume decorrelation for interferometric baselines of 500 m (top), 1000 m (middle), and 1500 m (bottom). The blue areas show additional errors due to the limited system accuracy (i.e. SNR, coregistration, quantization, etc.), and the red tubes indicate overall errors for different levels of temporal decorrelation (solid: $\gamma_{tmp}=0.8$, dashed: $\gamma_{tmp}=0.6$ dotted: $\gamma_{tmp}=0.4$). The assumed range of ground-to-volume ratios that can be addressed by varying polarisation (cf. Table 1) is marked by the darker areas of the error tubes. It becomes clear, that a reliable separation of the vertical phase centres is only possible for moderate levels of temporal decorrelation. Optimum performance for an inversion of the investigated Scots Pine forest scenario with a tree height of 20 m is predicted for perpendicular baselines in the order of 1km.

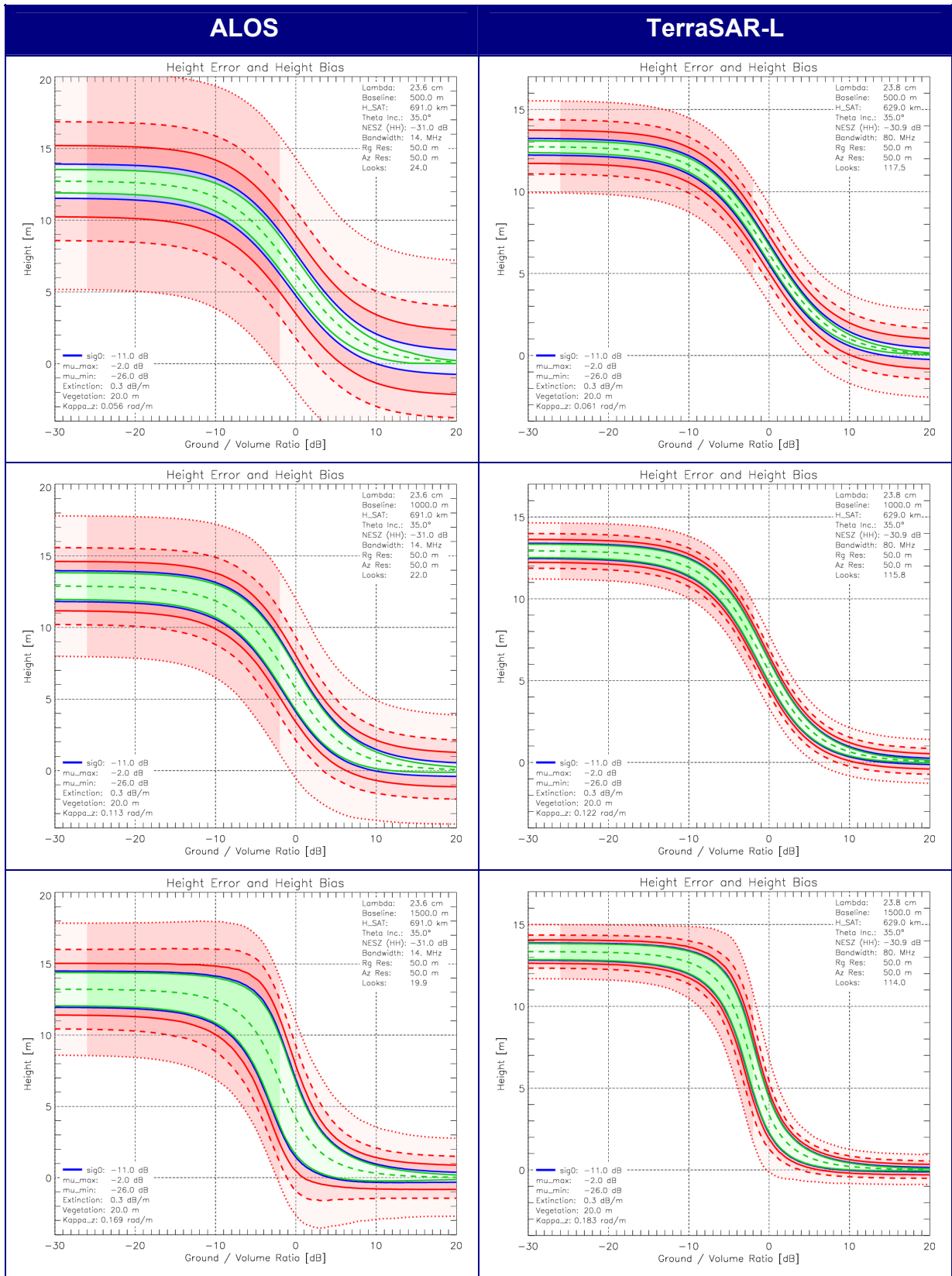


Fig. 1. Performance estimation for ALOS (left) and TerraSAR-L (right) repeat pass forest scenario with different interferometric baselines and an independent post-spacing of 50 m x 50 m. The baselines are 500 m (top), 1000 m (middle), and 1500 m (bottom). The volume height is 20 m, the extinction coefficient is 0.3 dB/m, and the incident angle is 35°. The indicated baselines are perpendicular to the line of sight. Green tubes show height errors due to volume decorrelation, blue tubes show additional errors due to the limited system accuracy, and red tubes indicate the total errors in case of temporal decorrelation (solid: $\gamma_{tmp}=0.8$, dashed: $\gamma_{tmp}=0.6$, dotted: $\gamma_{tmp}=0.4$). The expected range of ground-to-volume ratios ranging from -26 dB to -2 dB is indicated by the darker areas of the height error tubes.

3. SINGLE PASS MISSION SCENARIOS

Temporal decorrelation and atmospheric distortions limit the performance of conventional repeat pass interferometry. To avoid this, several spaceborne single pass InSAR concepts have been proposed and discussed over the last years [12]-[22]. Examples are single satellite boom concepts [13][14], satellite tandems ([12][18][22]), and multistatic satellite formations [16][17][19][20]. While most of these missions have been designed for a single polarisation mode, they can be extended/upgraded to provide fully polarimetric capabilities [23][10]. The following subsections discuss the different single-pass PolInSAR mission concepts.

3.1 Boom Concepts

One opportunity to acquire interferometric data in a single pass is the use of two antennas mounted on a single spacecraft. A prominent example for such a configuration is the Shuttle Radar Topography Mission (SRTM) which has been flown in February 2000 using a simultaneous data acquisition in C- and X-Band (cf. Fig. 2, [13][14]). SRTM was the first single pass SAR interferometer in space. Main mission objective was the acquisition of interferometric data for the generation of a consistent and accurate digital elevation model (DEM) for all land surfaces between $+60^\circ$ and -56° latitudes. This goal has been successfully achieved during the 11 day mission duration. Several extensions of this concept have been suggested in a recent ESA study [15]. A major limitation of the boom concept results from the relative short maximum possible mast length. The short interferometric baseline causes a low phase to height sensitivity which may in turn lead to a misbalance between volume and SNR decorrelation. Fig. 3 shows the predicted PolInSAR performance of potential L- and X-band boom interferometers. For illustration, we assumed in this simulation the system parameters for TerraSAR-L and TerraSAR-X (cf. 2nd and 5th column in Table 2). It becomes clear, that the performance is almost completely dominated by the limited system accuracy (blue tube), while the contributions from volume decorrelation have no significant influence (green tube). The SNR could e.g. be improved by increasing the transmit power, antenna gain, etc. and/or decreasing the orbit height. Lower altitudes would also improve the interferometric sensitivity due to the increased baseline angle. Note however, that long mission durations will require orbital altitudes of more than 400 km (SRTM: 233 km) to avoid excessive fuel consumption for atmospheric drag compensation. To alleviate the limitations due to the short baseline, the boom system may also be operated in a ping-pong interferometric mode, where the transmit antenna is switched from pulse to pulse. Assuming a simultaneous data acquisition by both antennas, this will yield two interferograms with two different baselines. Compared to SRTM, which used only a passive antenna at the outer tip of the mast, the maximum effective baseline is thus increased by a factor of two. Challenges in this simultaneous bistatic and monostatic data acquisition are the increased technological requirements for two fully active antennas as well as the increased susceptibility to ambiguities. To conclude, the low phase to height sensitivity of boom interferometers restricts their potential application area to the mapping of high vegetation layers with low extinction.

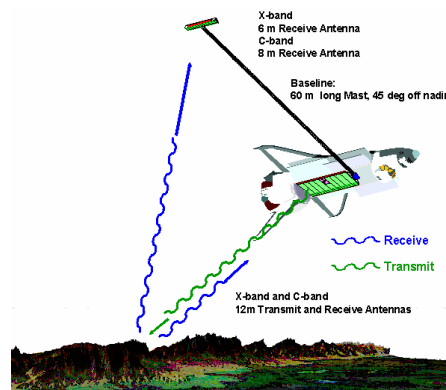


Fig. 2. Single pass SAR interferometry with one spacecraft (SRTM mission)

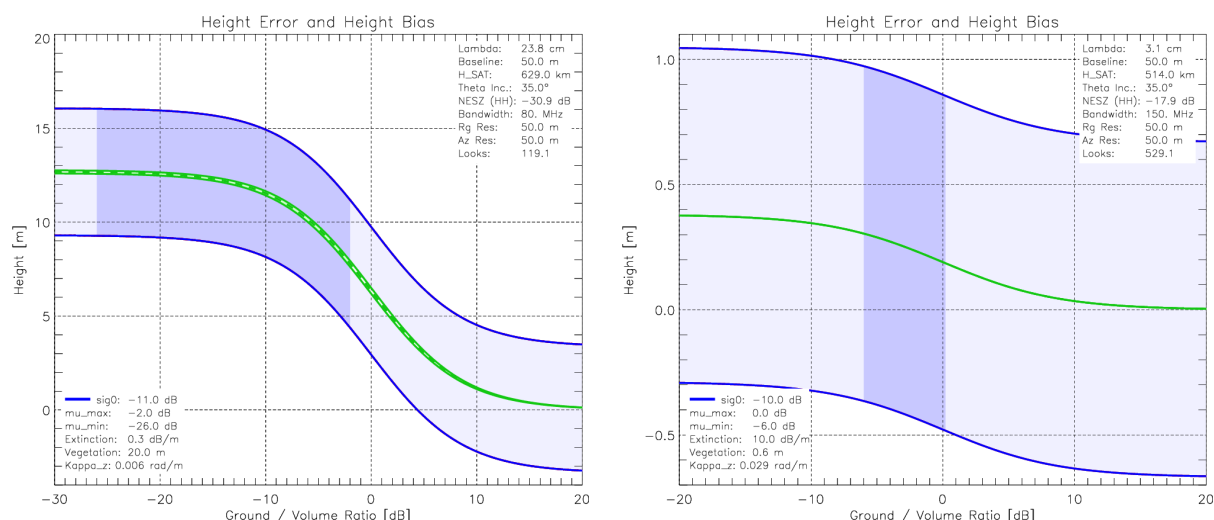


Fig. 3: Predicted PolInSAR performance for a potential L-band (left) and X-band (right) boom interferometer. The baseline is 100 m in bistatic or 50 m in ping pong mode. The independent post-spacing is 50 m x 50 m. System parameters correspond to TerraSAR-L and TerraSAR-X (cf. 2nd and 5th column in Table 2).

3.2 Fully Active Interferometric Satellite Constellations

Fully active SAR constellations use two or more conventional radar satellites flying in close formation to acquire interferometric data during a single pass. Examples for fully active SAR constellations are twin satellite formations like the Radarsat 2/3 tandem [18] or TanDEM-X [22], as well as multi-satellite constellations like the Technology Satellite of the 21st century (TechSAT21, [16]). All these formations provide a highly reconfigurable radar system with flexible imaging geometry, thereby enabling an interferometric operation in either pursuit monostatic or simultaneous bistatic mode [18][22]. In the following, we will consider the performance of several twin satellite configurations for different applications at L-, C-, and X-band.

The blue tubes in Fig. 1 may be regarded as first approximations for the achievable performance of a potential TerraSAR-L and ALOS tandem configuration in case of forest mapping. Note that the indicated interferometric baselines should be multiplied by a factor of two in case of operating the system in bistatic mode. It becomes clear, that an excellent performance may be achieved for a high bandwidth system like TerraSAR-L, where the separation of the vertical phase centres becomes as large as 8 times the phase error standard deviation.

For the investigation of a potential Radarsat 2/3 [18] or TerraSAR-X tandem [22], we consider the mapping of agriculture fields as promising PolInSAR applications (cf. right columns in Table 1). Since such applications will in general require a finer horizontal resolution, we assume now an independent post-spacing of 30 m x 30 m. Fig. 5 shows the predicted performance for the Radarsat 2/3 tandem operating in the nominal 30 MHz mode (left) and in a hypothetical 100 MHz mode (right). A baseline of 2000 m has been chosen in this example where we assumed an operation in pursuit monostatic mode. The selected baseline is almost optimal for a bandwidth of 30 MHz. By comparing the left and right plots in Fig. 5, it becomes evident that a higher bandwidth is in general of great advantage to reduce the contributions from the different error sources (the only exception are phase errors from the SNR which remain –in first approximation– constant due to the rise of the NESZ with higher bandwidth). Note that a higher bandwidth would also enable an increase of the interferometric baseline, thereby further reducing the height errors in this example with low vegetation height.

Fig. 6 shows the predicted performance of a TerraSAR-X tandem (TanDEM-X, [22]) for two different interferometric baselines of 1000m (left) and 4000m (right) assuming an operation in pursuit monostatic mode with 150 MHz range bandwidth. The accuracy is mainly limited by the system noise in case of small baselines (left), while volume decorrelation becomes the dominant error source for large baselines (right). Note that the high resolution of TerraSAR-X enables a large number of independent looks, thereby allowing for an efficient reduction of the different errors.

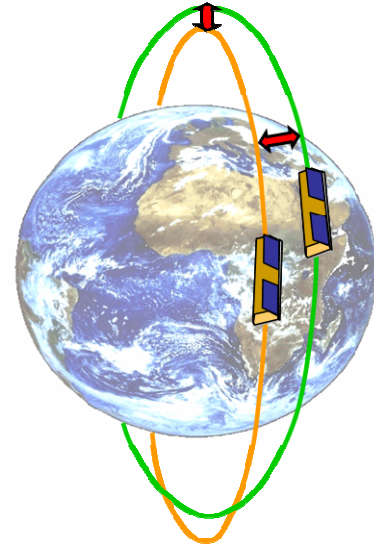


Fig. 4. Single pass interferometry with satellite tandem in HELIX formation.

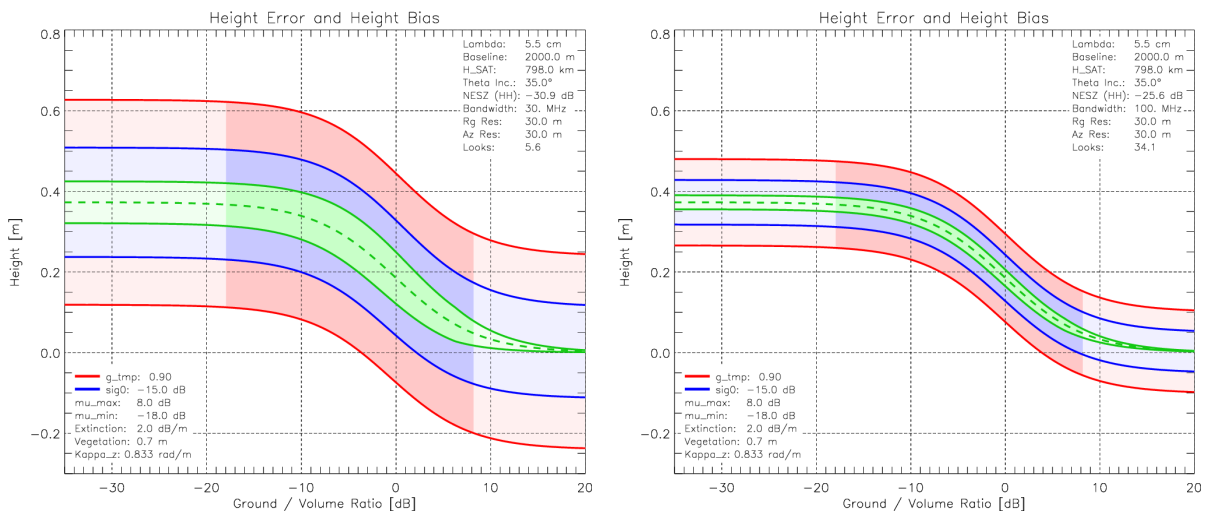


Fig. 5: PolInSAR performance for the C-band agriculture scenario with Radarsat 2 in standard 30 MHz mode (left) and hypothetical 100 MHz mode (right). The independent post-spacing is 30 m x 30 m and the baseline is 2000 m assuming pursuit monostatic mode. The red tubes indicate additional errors in case of residual temporal decorrelation with $\gamma_{tmp}=0.9$.

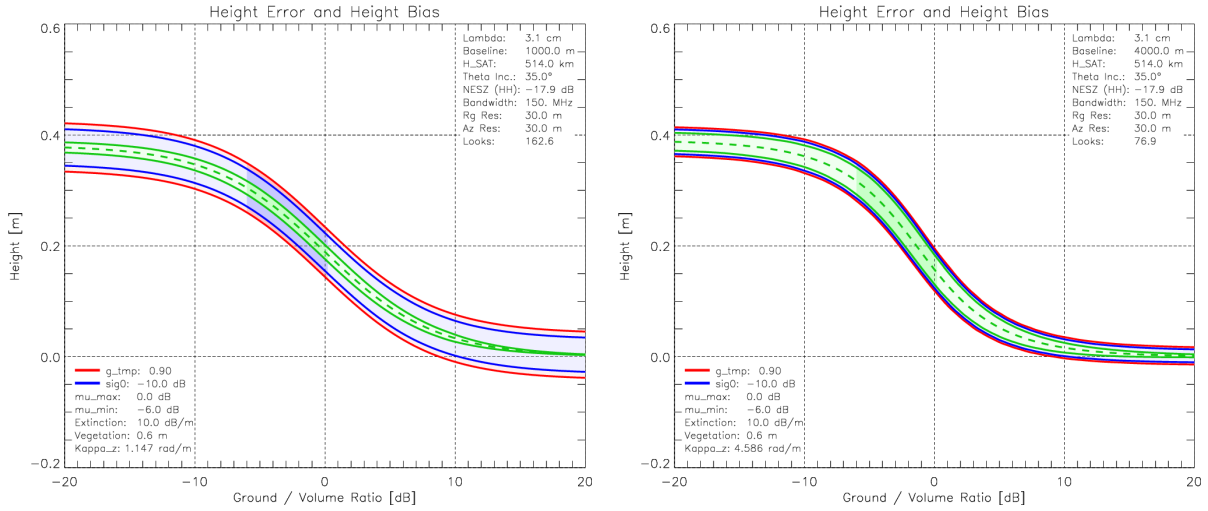


Fig. 6: PolInSAR performance for the X-band agriculture scenario with TanDEM-X. The baselines are 1000 m (left) and 4000 m (right) assuming an operation in pursuit monostatic mode. The bandwidth is 150 MHz and the independent post-spacing is 30 m x 30 m. The red tubes indicate errors for temporal decorrelation with $\gamma_{tmp}=0.9$.

3.3 Semi-Active Satellite Formations

Semi-active satellite formations use multiple passive receivers in combination with one active radar illuminator. Passive receivers enable a cost-efficient implementation of a single-pass SAR interferometer since the low power demands and the use of deployable antennas will allow for an accommodation of the payload on low-cost microsatellites. First suggestions for such semi-active interferometric SAR missions were the Interferometric Cartwheel [17] and its polarimetric extension as in the joint CNES/DLR VOICE proposal [23]. Alternative constellations have been suggested in [19][20].

In the following, we will illustrate the achievable performance for such a semi-active fully polarimetric and interferometric SAR constellation. As an example, we assume an illumination by the TerraSAR-L satellite. The parameters of the passive receivers have been taken from [21][20] (reflector antennas with a diameter of 3 m, Rx noise figure of 2.5 dB, Rx+proc. losses: 2 dB). Fig. 7 shows the predicted PolInSAR performance for the Scots Pine forest scenario mapped with an interferometric baseline of 1500 m. The independent post-spacing is 50 m x 50 m (left) and 30 m x 30 m (right). The red tubes indicate again additional errors in case of residual temporal decorrelation with $\gamma_{tmp}=0.9$. Small amounts of temporal decorrelation could be due to a relative along-track displacement between the passive receivers, which causes a short delay in the iso-Doppler mapping of the interferometric image pair. It is clear, that an excellent performance can be achieved, which is only slightly inferior to the performance of a fully active L-band tandem configuration. A great advantage of the semi-active system is its potential to provide multiple interferometric baselines in a single pass by increasing only the

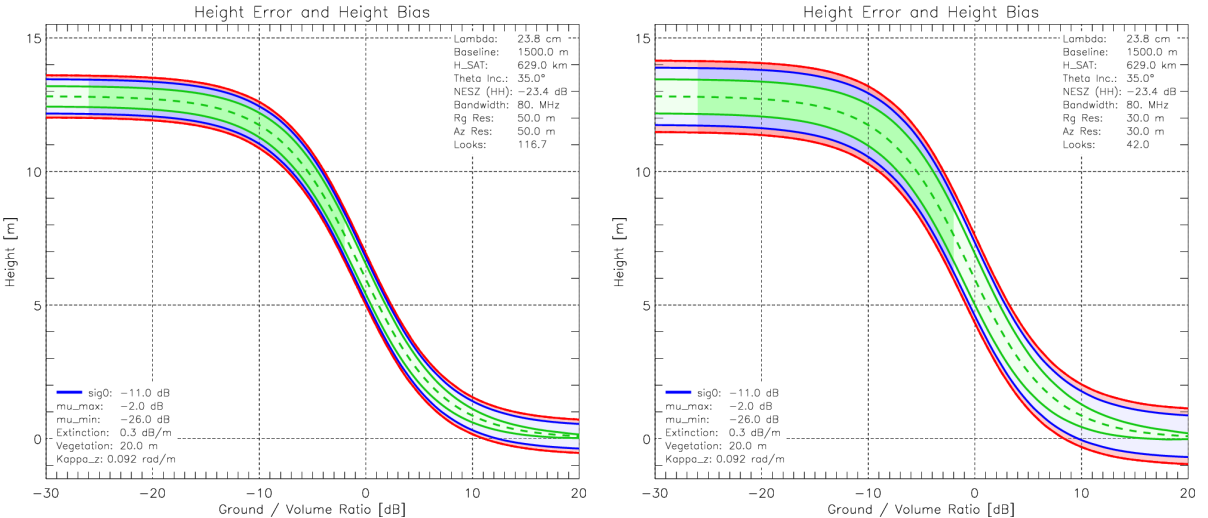


Fig. 7: PolInSAR performance for the L-band forest scenario with a semi-active satellite formation for an independent post-spacing of 50m x 50m (left) and 30m x 30m (right). The baseline is 1500m (bistatic mode). The red tubes indicate additional errors in case of residual temporal decorrelation with $\gamma_{tmp}=0.9$.

number of low-cost passive receivers. For example, the satellite formation in Fig. 8 (Trinodal Pendulum) provides three interferometric baselines with a fixed baseline ratio. Different baselines are of great advantage to achieve optimum system performance for different vegetation heights and a joint evaluation of multiple baselines provides important additional information about the vertical structure of volume scatterers.

An important issue arises from the small antennas of the passive receivers. The reduced antenna size is a prerequisite for an accommodation of all receiver satellites in a common launcher. The antenna size and its shape are further limited by the maximum momentum that can be handled by microsattellites [21]. The short antenna length of the passive receiver satellites will cause an azimuth antenna pattern with a broad mainlobe. Hence, the level of the azimuth sidelobes in the joint antenna pattern will be substantially increased, thereby increasing also the required PRF for unambiguous SAR imaging. To alleviate this effect, three different tapering functions for TerraSAR-L have been investigated in [20]: (1) Taylor, (2) Hamming, and (3) Dolph-Tschebyscheff tapering. Fig. 9 shows the azimuth ambiguity to signal ratio as a function of the PRF for constant tapering (red), Taylor tapering (yellow), Hamming tapering (green), and Dolph-Tschebyscheff tapering (blue) at a processed bandwidth of 1,0 kHz (dashed) and 1,2 kHz (solid). It is clear, that

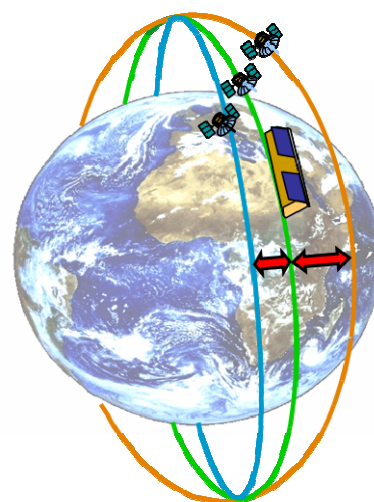


Fig. 8. Semi-active satellite formation (Trinodal Pendulum).

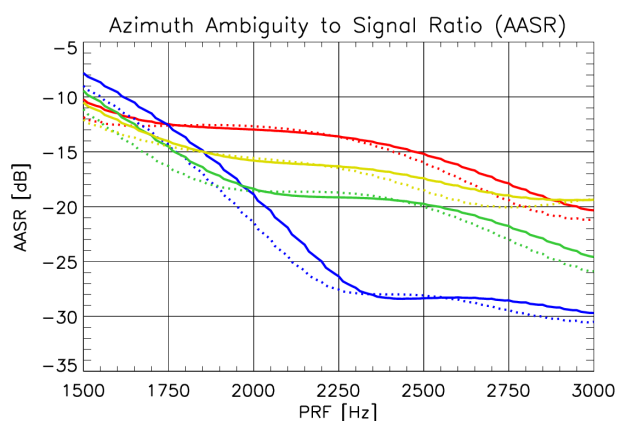


Fig. 9: Azimuth ambiguities as a function of the PRF for constant (red), Taylor (yellow), Hamming (green), and Dolph-Tschebyscheff (blue) tapering with a processed Doppler bandwidth of 1 kHz (dotted) and 1.2 kHz (solid).

will become rather small for higher incident angles. Wide swath imaging requires hence an operation with steep incident angles or an increase of the antenna size (e.g. in the transmitter). A potential alternative is the use of innovative ambiguity suppression techniques [24].

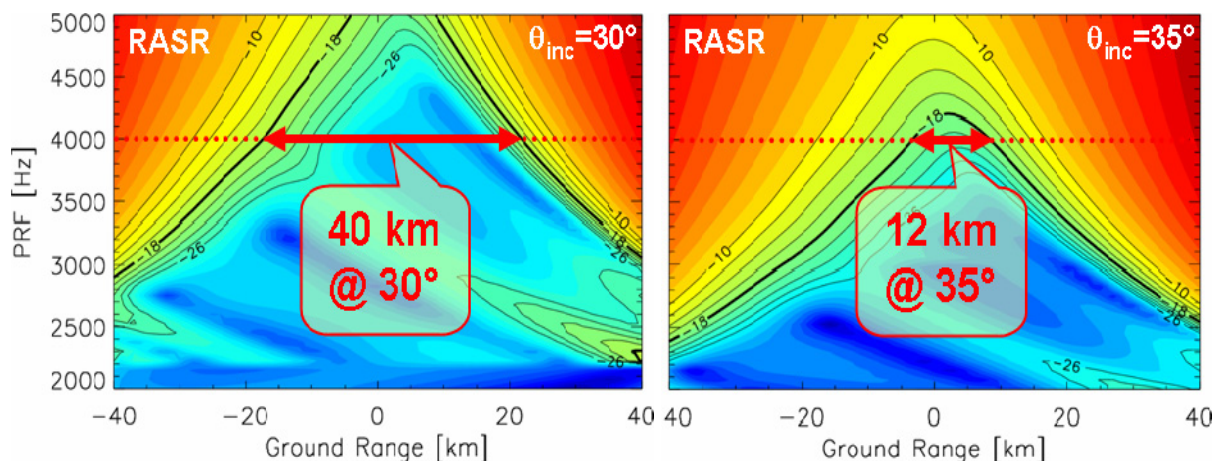


Fig. 10: Range ambiguity to signal ratio (RASR) as a function of swath position and PRF for incident angles of 30° (left) and 35° (right).

4. DISCUSSION

We have analysed the potential of several spaceborne mission scenarios to acquire polarimetric and interferometric SAR data for the accurate retrieval of forest and agriculture parameters. It has been shown that the expected performance of repeat-pass missions is severely affected by even moderate levels of temporal decorrelation. Hence, a large number of looks would be required to achieve a sufficient separation of the vertical phase centres at the different polarisations. This raises also the question, whether temporal errors are adequately described by a simple coherence loss in a multiplicative coherence model. The predicted improvement by multilooking is based on the implicit assumption that temporal errors correspond to independent additive white Gaussian noise in each complex SAR image. Such an implicit assumption could for example be violated by inhomogeneities or by taking into account the effects of precipitation and wind which may cause spatially correlated and polarisation dependent shifts of the phase centres. An effective means to reduce temporal errors in a repeat pass scenario is the selection of orbits with shorter repeat cycles. However, shorter repeat cycles cause larger gaps between the satellite ground tracks, thereby requiring a wide range of incident angles to achieve full coverage especially in equatorial regions. The acquisition of fully polarimetric data over a wide range of incident angles is in turn in conflict with range and azimuth ambiguities. Hence, either large antennas or new multichannel data acquisition techniques [24] have to be used to acquire unambiguous SAR data over a wide image swath.

Further challenges arise from wave propagation errors. Faraday rotation in the ionosphere may cause significant differences between measured and actual scattering matrices. This nonreciprocal rotation of the polarisation plane depends strongly on the wavelength and becomes up to several 10^{th} of degrees in L-band at maximum solar activity [25]. Faraday rotation is of special concern in repeat pass mission scenarios due to the probably different rotation angles during subsequent satellite passes. The impact of Faraday rotation on single-pass PolInSAR mission scenarios is presumably less critical, since the rotation of the polarisation plane will be (almost) equal for all interferometric channels, thereby preserving the relative polarisation state within each interferometric channel. A calibration technique for conventional linearly polarized polarimetric SAR data subject to Faraday rotation has been suggested and discussed in [26]. Note that a potential calibration for different amounts of Faraday rotations between subsequent satellite passes could also take advantage of the coherent data acquisition by optimizing the interferometric coherence. The impact of residual uncalibrated errors due to Faraday rotation has still to be analysed in detail taking into account the varying requirements for the different application scenarios. Another source for wave propagation errors are atmospheric disturbances which will cause a delay of the signal that manifests itself as a space-variant interferometric phase shift in case of repeat pass data acquisitions. This phase shift has high spatial correlation [26], thereby introducing a low frequency bias in the phase of all polarimetric channels which will mainly affect estimates of the ground topography phase while leaving the residual PolInSAR parameters untouched. Note that the impact of atmospheric phase errors will become more severe for shorter wavelengths if we assuming an interferometric system with a fixed height of ambiguity (i.e. a fixed vertical wavenumber k_z).

Another aspect relates to the selection and estimation of satellite orbits. The analyses in this paper demonstrated the dependency of the PolInSAR performance on both the vegetation height and the length of the interferometric baselines. Small baselines are well suited to avoid phase ambiguities in case of high vegetation layers while large baselines allow for an improved accuracy in areas with lower vegetation. The selection of optimized orbits requires hence some a priori knowledge about the scene to be imaged, or, as an alternative, a simultaneous data acquisition with multiple baselines as provided e.g. by the Trinodal Pendulum (cf. Fig. 8). Orbit estimation errors will mainly affect measurements of the ground topography phase, but could also introduce a bias in the inversion of PolInSAR models due to the use of a wrong interferometric baseline length. Single pass configurations have the advantage that they enable a very precise 3-D baseline estimation with mm accuracy based on a double difference evaluation of GPS carrier phase measurements [28]. Furthermore, the impact of baseline errors is reduced by a factor of two in bistatic systems with the same vertical wavenumber. This is due to the fact that such configurations require twice the baseline length for the same phase to height scaling. On the other hand, the impact of oscillator errors becomes significantly more severe in bistatic configurations due to the missing cancellation of low frequency phase noise as in a monostatic system where both the transmitter and the receiver use the same oscillator signal. Hence, an appropriate phase synchronisation will be required for precise estimates of the ground topography phase, while the demands for the estimation of other PolInSAR parameters are less critical. Further challenges could arise from the calibration of semi-active bistatic SAR systems, which may require the employment of new calibration techniques due to the bistatic angle associated with large transmitter-receiver separations. Notwithstanding these challenges, single-pass SAR interferometers in either pursuit monostatic or bistatic mode are the only means to overcome the inherent limitations from repeat pass SAR interferometry. By this, they enable precise and uncorrupted polarimetric and interferometric measurements of volume scatterers for a broad spectrum of powerful remote sensing applications.

5. ACKNOWLEDGEMENT

This work has been supported by the European Space Agency (Polarimetric and Interferometric Mission and Application Study, Contract No. 17893/03/I-LG).

6. REFERENCES

- [1] Cloude S.R. and Papathanassiou K.P., Polarimetric SAR Interferometry, *IEEE Transactions on Geoscience and Remote Sensing*, Vol. 36, No. 5, pp. 1551-1565, 1998.
- [2] Papathanassiou K.P. and Cloude S.R., Single Baseline Polarimetric SAR Interferometry, *IEEE Transactions on Geoscience and Remote Sensing*, Vol. 39, No. 11, pp. 2352-2363, 2001.
- [3] Cloude S.R., Corr D.G., Williams M.L., Target Detection Beneath Foliage Using Polarimetric SAR Interferometry, *Waves in Random Media*, Vol. 14, No. 2, pp. S393 - S414, 2004.
- [4] Macelloni G., Paloscia S., Pampaloni P., Marliani F., Gai M., The relationship between the backscattering coefficient and the biomass of narrow and broad leaf crops, *IEEE Trans. Geosci. Remote Sens.*, Vol. 39, No. 4, pp. 873-884, 2001.
- [5] ONERA simulations carried out under ESA contract ESTEC 16924/02/NL/LvH
- [6] Brown S.C.M., Quegan S., Morrison K., Bennett J.C., Cookmartin G., High Resolution Measurements of Scattering in Wheat Canopies-Implications for Crop Parameter Retrieval, *IEEE Trans. GRS*, Vol. 41, No. 7, pp 1602-1610, 2003.
- [7] Ulaby F. and Dobson C., *Handbook of Radar Scattering Statistics for Terrain*, Artech House, Norwood, MA, 1989.
- [8] Ulaby F., Moore R.T., Fung A.K., *Microwave Remote Sensing: Active and Passive*, pp. 1558-1571, Artech House, 1986.
- [9] Rodriguez E. and Martin J.M., Theory and Design of Interferometric Synthetic Aperture Radars, *IEE Proceedings-F*, Vol. 139, No. 2, pp. 147-159, 1992.
- [10] Krieger G., Papathanassiou K. and Cloude S., Spaceborne Polarimetric SAR Interferometry: Performance Analysis and Mission Concepts, to appear in *EURASIP Journal on Applied Signal Processing: Special Issue on Advances in Interferometric Synthetic Aperture Radar Processing*, 2005.
- [11] Polarimetric and Interferometric Mission and Application Study, ESA Contract No. 17893/03/I-LG
- [12] Zebker H.A., Farr T.G., Salazar R.P., and Dixon T.H., Mapping the World's Topography Using Radar Interferometry: The TOPSAT Mission, *Proc. IEEE*, Vol. 82, No. 12, pp. 1774-1786, 1994.
- [13] Rosen P.A., Hensley S., Joughin I.R., Li F.K., Madsen S.N., Rodriguez E., Goldstein R., Synthetic Aperture Radar Interferometry, *Proc. IEEE*, Vol. 88, No. 3, pp. 333-382, 2000.
- [14] Werner M., Shuttle Radar Topography Mission (SRTM): Mission Overview, *Journal of Telecommunication (Frequenz)*, Vol. 55, No. 3-4, pp. 75-79, 2001.
- [15] New Techniques for Simultaneous SAR Interferometry, ESA Contract Nr. 16100/02/NL/EC, 2003.
- [16] Martin M., Klupar P., Kilberg S., Winter J., TechSat 21 and Revolutionizing Space Missions Using Microsatellites, American Institute of Aeronautics and Astronautics, 2001.
- [17] Massonnet, D., Capabilities and Limitations of the Interferometric Cartwheel, *IEEE Trans. Geosci. Remote Sensing*, Vol. 39, No. 3, pp. 506-520, 2001.
- [18] Evans N.B., Lee P., and Girard R., The Radarsat 2&3 Topographic Mission: An Overview, Proceedings IGARSS'02 (CD-Rom), Toronto, Canada, 22-26 June 2002.
- [19] Krieger G., Fiedler H., Mittermayer J., Papathanassiou K., Moreira A., Analysis of Multistatic Configurations for Spaceborne SAR Interferometry, *IEE Proc. Radar Sonar Navigation*, Vol. 150, No. 3, pp. 87- 96, 2003.
- [20] Zink M., Krieger G., Amiot T., Interferometric Performance of a Cartwheel Constellation for TerraSAR-L, Fringe Workshop, Frascati, Italy, 2003.
- [21] Amiot T., Krieger G., Douchin F., Werner M., Fjortoft R.: TerraSAR-L Interferometric Cartwheel : DEM Performance Estimation. Radar Conference, Toulouse, 18-22 October 2004.
- [22] Moreira A. et al., TanDEM-X: TerraSAR-X Add-on for Digital Elevation Measurements, IGARSS 04, Anchorage, USA, 2004.
- [23] Massonnet D., Moreira A., Bamler R., Souyris J.C., Voice: Volumetric Interferometry Cartwheel Experiment, Proposal for a mission to retrieve globally vegetation structure parameters and above ground forest biomass using a passive polarimetric SAR interferometry Cartwheel configuration. January, 8th, 2002.
- [24] Krieger G., Gebert N., Moreira A.: Unambiguous SAR Signal Reconstruction from Nonuniform Displaced Phase Center Sampling. *IEEE Geoscience and Remote Sensing Letters*, Vol. 1, No. 4, pp. 260-264, 2004.
- [25] Wright P., Quegan S., Wheadon N., Hall C.D., Faraday Rotation Effects on L-Band Spaceborne SAR Data, *IEEE Trans. Geoscience Remote Sensing*, Vol. 41, No. 12, pp. 2735-2744, 2003.
- [26] Freeman A., Calibration of Linearly Polarized Polarimetric SAR Data Subject to Faraday Rotation, *IEEE Trans. Geoscience Remote Sensing*, Vol. 42, No. 8, pp. 1617-1624, 2004.
- [27] Hanssen, R.F., *Radar Interferometry – Data Interpretation and Error Analysis*, Kluwer Academic Press, Dordrecht, 2001.
- [28] Leung S., Montenbruck O., Real-Time Navigation of Formation-Flying Spacecraft Using Global Positioning System Measurements, submitted to *Journal of Guidance, Control, and Dynamics*, 2004.